Estimation of the Hurst Exponent of Noisy or Blurred Fractal Textures. Application to Computer-Aided Mammogram Analysis.

B. Pascal[1], C. Launay[2], H. Biermé[3]

1. Nantes Université, École Centrale Nantes, CNRS, LS2N, UMR 6004, F-44000 Nantes, France barbara.pascal@cnrs.fr
2. Université Bretagne Sud, CNRS LMBA, UMR 6205, F-56000, Vannes, France claire.launay@univ-ubs.fr
3. Université de Tours, Université d'Orléans, CNRS, IDP, UMR 7013, F-37200, Tours, France hermine.bierme@univ-tours.fr

Context, aims and contributions

One over eight women will be diagnosed with *breast cancer* in her lifetime. Survival is greatly improved by *early detection*. This motivates upstream assessment of *cancer risk*, so that women at higher risk undergo mammograms more frequently. To that aim, fatty vs. dense vs. *disrupted* breast tissues are discriminated through the *fractal attributes* of mammographic textures (Marin *et al.*, 2017, *Med. Phys.*; Gerasimova-Chechkina *et al.*, 2021, *Front. Physiol.*).

Challenge: The presence of *noise* and/or *blur* in real mammograms significantly impairs accuracy and robustness of fractal attribute estimators.

Contributions: Mammographic textures are characterized through their *Hurst exponent* $H \in (-1,1)$, a widely used fractal attribute,

- *sensitivity* to noise and blur of two state-of-the-art estimators of H quantified on different synthetic texture models;
- estimation of Hurst exponent H on real mammograms from the VinDr-Mammo dataset (Nguyen, 2023, *Scientific Data*).

Outcome: *Overestimation* of the Hurst exponent of dense tissues from old datasets; suspect *model mismatch* or *lack of robustness* to population shift.

Isotropic texture models

Gray-scale texture: *stochastic* $\mathsf{F} : \Omega \subset \mathbb{R}^2 \to \mathbb{R}$

Hurst exponent: $\mathsf{F}^{\underline{\delta}}(\underline{x}) = \mathsf{F}(\underline{x}+\underline{\delta}) - \mathsf{F}(\underline{x})$, $\underline{\delta} \in \mathbb{R}^2$

$$\mathbb{E}\left[\mathsf{F}^{\underline{\delta}}(\underline{x}+\underline{h})\mathsf{F}^{\underline{\delta}}(\underline{x})\right] \underset{\|\underline{h}\|\to\infty}{=} c\|\underline{h}\|^{2H-2} + o\left(\|\underline{h}\|^{2H}\right)$$

$\Longrightarrow$ F has *Hurst exponent* equal to H.

Fractional Brownian field: $\alpha \in (0,1)$

$$\mathsf{B}_\alpha(\underline{x}) = \int_{\mathbb{R}^2} (\mathrm{e}^{-\mathrm{i}\underline{x}\cdot\underline{\omega}} - 1)\|\underline{\omega}\|^{-\alpha-1}\,\mathrm{d}\widetilde{\mathsf{W}}(\underline{\omega})$$

$\Longrightarrow$ *historical* model with $H = \alpha$.

Stationary self-similar fields

Fractional Gaussian field: $\alpha \in (0,1)$

$$\mathsf{G}_\alpha(\underline{x}) = \mathsf{B}_\alpha(\underline{x}+\underline{e}_1) + \mathsf{B}_\alpha(\underline{x}+\underline{e}_2) - 2\mathsf{B}_\alpha(\underline{x})$$

(Pascal *et al.*, 2021, *Appl. Comput. Harm. Anal.*)

Filtered fractional Brownian field:

$\mathsf{C}_\alpha(\underline{x}) = \langle \mathsf{B}_\alpha, \mathsf{u}_{\underline{x}} \rangle$, $\alpha \in (0,1)$, u radial filter

u: above scale 2^3 (Pascal *et al.*, 2025, *SSP*)

Both G_α and C_α satisfy $H = \alpha - 1$.

H-self-similarity: fractal property

$$\forall c > 0, \quad \{\mathsf{F}(c\underline{x}); \underline{x} \in \mathbb{R}^2\} \overset{(\text{law})}{=} c^H \{\mathsf{F}(\underline{x}); \underline{x} \in \mathbb{R}^2\}$$

Examples: $\alpha_\mathsf{f} = 0.3$ (*top*) and $\alpha_\mathsf{d} = 0.65$ (*bottom*)

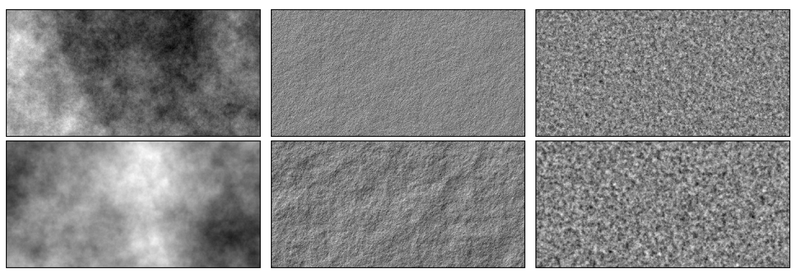

fBf B_α fGf G_α filtered fBf C_α

In practice:

- textured images of $N = 512 \times 512$ pixels
- generated with the turning-band method (Biermé *et al.*, 2015, *J. Comput. Graph. Stat*)
- normalized: zero mean & unit variance

Two wavelet-based estimators of the Hurst exponent

Wavelet leaders: 2D wavelet coefficients $Y_\mathsf{F}^{(m)}(j,\underline{k}) = 2^{-j}\langle \mathsf{F}, \psi_{j,\underline{k}}^{(m)} \rangle$ from $\left\{\psi_{j,\underline{k}}^{(m)},\ m = 1,2,3,\ j = j_1, ..., j_2,\ \underline{k} \in \mathbb{Z}^2\right\}$, orientation m, octave j, location $\underline{x} = 2^j\underline{k}$

Leaders: $\mathcal{L}_{j,\underline{k}} = \sup_{\substack{\lambda_{j',\underline{k}'} \subset 3\lambda_{j,\underline{k}} \\ m \in \{1,2,3\}}} |2^{j(1+\gamma_{\text{int}})} Y_\mathsf{F}^{(m)}(j',\underline{k}')|$; $\lambda_{j,\underline{k}} = [\underline{k}2^j, (\underline{k}+1)2^j)$ with $3\lambda_{j,\underline{k}} = \bigcup_{\underline{p}\in\{-1,0,1\}^2} \lambda_{j,\underline{k}+\underline{p}}$ (Jaffard *et al.*, 2006, *Wavelet Anal. App.*)

Structure functions: $\mathcal{S}_{j,q} = K_j^{-1} \sum_{\underline{k}\in\mathbb{Z}|2^j\underline{k}\in\Omega} \left(\mathcal{L}_{j,\underline{k}}\right)^q \sim 2^{jq(H+\gamma_{\text{int}})}$; let $\upsilon_{q,p} = \sum_{j=j_1}^{j_2} (jq)^p$ for $p \in \{0,1,2\}$

Leader-based estimator

$$\widehat{H}_q^{\mathsf{lead}} = \frac{\upsilon_1 \sum_{j=j_1}^{j_2} \log \mathcal{S}_{j,q} - \upsilon_{q,0} \sum_{j_1}^{j_2} jq \log \mathcal{S}_{j,q}}{q\left(\upsilon_{q,1}^2 - \upsilon_{q,2}\upsilon_{q,0}\right)} - \gamma_{\text{int}}$$

In practice:

- Daubechies wavelets from $j_1 = 2$ to $j_2 = 5$
- $n_\psi = 2$ vanishing moments, $q = 2$
- fractional integration $\gamma_{\text{int}} = 2$
- use WLMBF toolbox (Wendt *et al.*, 2009, *Signal Process.*)

Monogenic wavelets: 2D Riesz transform $\mathcal{F}\left(\mathcal{R}_\ell \mathsf{F}\right)(\underline{\xi}) = -i\frac{\xi_\ell}{\|\underline{\xi}\|}\mathcal{F}\left(\mathsf{F}\right)(\underline{\xi})$, $\ell \in \{1,2\}$ $\mathcal{F}$: 2D Fourier (Stein, 1993, *Princeton Univ. Press*)

Monogenic signal: radial function u at octave 0, for $j \geq 1$, $\mathsf{u}_{j,\underline{n}}(\underline{x}) = 2^{-j}\mathsf{u}(2^{-j}(\underline{x}-\underline{n}))$

multiscale decomposition of F through u: $\mathcal{M}\mathsf{F}(\mathsf{u}_{j,\underline{n}}) = \left(\langle \mathsf{F}, \mathsf{u}_{j,\underline{n}} \rangle, \langle \mathcal{R}_1\mathsf{F}, \mathsf{u}_{j,\underline{n}} \rangle, \langle \mathcal{R}_2\mathsf{F}, \mathsf{u}_{j,\underline{n}} \rangle\right)$

$A_{j,\underline{n}}^2 = \|\mathcal{M}\mathsf{F}(\mathsf{u}_{j,\underline{n}})\|^2$: $\mathbb{E}(A_{j_2,\underline{n}}^2)/\mathbb{E}(A_{j_1,\underline{n}}^2) = 2^{2(j_2-j_1)(H+1)}$; estimate: $\widehat{A_j^2} = N^{-1} \sum_{\underline{n}\in\Omega\cap\mathbb{Z}^2} \|\mathcal{M}\mathsf{F}(\mathsf{u}_{j,\underline{n}})\|^2$

Monogenic wavelet-based estimator

$$\widehat{H}^{\mathsf{monog}} = \frac{1}{2\log(2)(j_2-j_1)} \log\left(\widehat{A_{j_2}^2}/\widehat{A_{j_1}^2}\right) - 1$$

In practice:

- u high-pass filter: 2 vanishing moments
- use Image Monogenic Analysis toolbox
- analysis between octaves $j_1 = 3$ and $j_2 = 4$

(Biermé *et al.*, 2025, *Appl. Comput. Harmon. Anal.*)

Numerical experiments

Robustness of Hurst exponent estimators: noisy *or* blurred synthetic textures, $\mathsf{F} \in \{\mathsf{B}_\alpha, \mathsf{G}_\alpha, \mathsf{C}_\alpha\}$

$\widetilde{\mathsf{F}}(\underline{n}) = (\mathsf{g}_\delta \star \mathsf{F})(\underline{n}) + \sigma\xi_{\underline{n}}$, noise variance $\sigma^2 \in [10^{-4}, 10^2]$, blur length $\delta \in [10^{-3}, 10^4]$

$(\xi_{\underline{n}})_{\underline{n}\in\Omega\cap\mathbb{Z}^2}$ *i.i.d. standard Gaussian* variables, g_δ *Gaussian kernel* of typical length δ.

Averaged $\widehat{H}^{\mathsf{lead}}$ and $\widehat{H}^{\mathsf{monog}}$ with 95% Gaussian confidence interval estimated on 20 texture realizations:

- $\widehat{H}^{\mathsf{lead}}$ and $\widehat{H}^{\mathsf{monog}}$ systematically agree precisely for all models, regularities, noise and blur levels;
- at small noise *or* blur level, accurate estimation of H;
- as noise level σ^2 increases, H estimates tend to white noise Hurst exponent $H_{\mathsf{wn}} = -1$;
- as blur length δ increases, reach $H_{\mathsf{smooth}} = 2$, number of vanishing moments for both estimators.

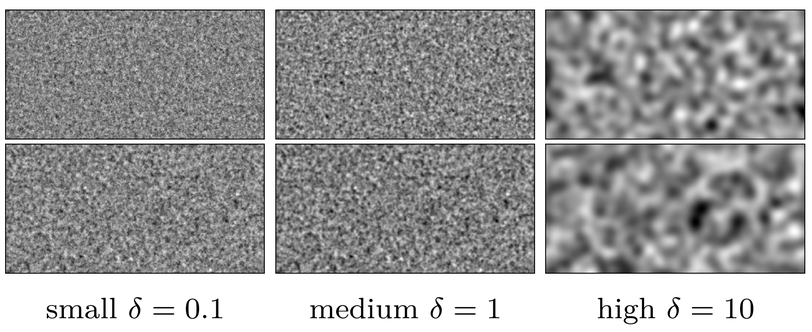

small $\delta = 0.1$ medium $\delta = 1$ high $\delta = 10$

Extreme blur $\delta = 10^4$ matching $H_{\mathsf{smooth}} = n_\psi$.

	B_α	G_α	C_α
$\widehat{H}^{\mathsf{lead}}$	2.09 ± 0.01	2.10 ± 0.02	1.83 ± 0.02

Real mammograms analysis: extracted from the public VinDr-Mammo dataset

$P = 20$ patches of $N = 512 \times 512$ pixels from *fatty*, BI-RADS A, vs. *dense*, BI-RADS D, mammograms

- at extreme noise (resp. blur) level $H_{\mathsf{wn}} = -1$ (resp.$H_{\mathsf{smooth}} = 2$) reached;
- for *fatty* mammograms, estimated H similar to $\mathsf{B}_{\alpha_\mathsf{f}}$, $\alpha_\mathsf{f} = 0.3$; (Marin *et al.*, 2017, *Med. Phys.*)
- for *dense* mammograms, estimated H departs from *all* $\mathsf{B}_{\alpha_\mathsf{d}}$, $\mathsf{G}_{\alpha_\mathsf{d}}$,$\mathsf{C}_{\alpha_\mathsf{d}}$, with reported $\alpha_\mathsf{d} = 0.65$;
- *fatty* and *dense* mammograms have the *same* estimated Hurst exponents, contradicts literature!

Synthetic textures Real mammograms

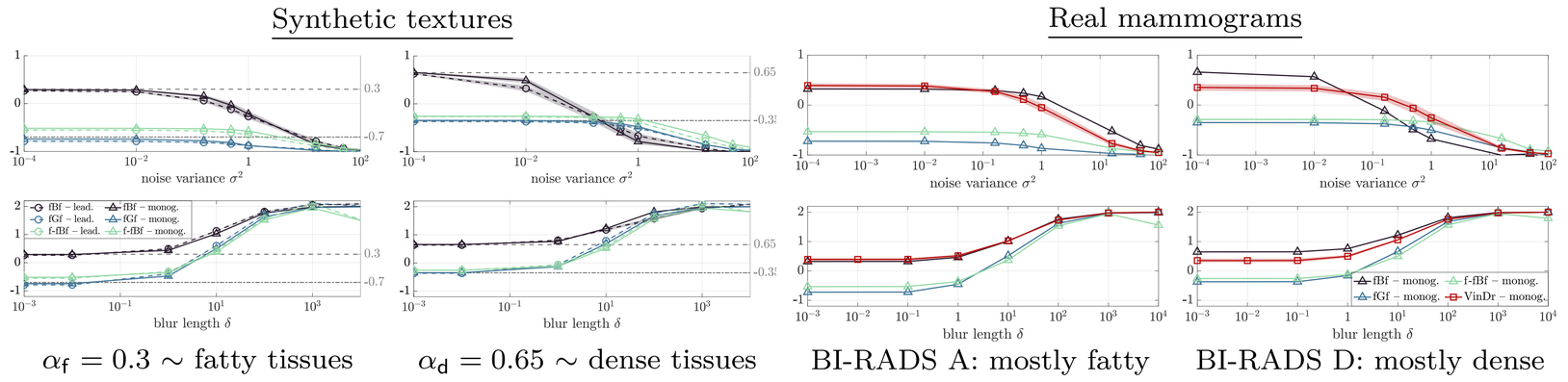

$\alpha_\mathsf{f} = 0.3 \sim$ fatty tissues $\alpha_\mathsf{d} = 0.65 \sim$ dense tissues BI-RADS A: mostly fatty BI-RADS D: mostly dense

Conclusions & perspectives

- *Quantification* of under-(resp over-)estimation of the Hurst exponent in the presence of noise (resp. blur) on several *synthetic* texture models;
- Experiments on *real* mammograms showed a mismatch with Hurst exponent values for *dense* tissues reported in the literature;

universality of *isotropic* models?
robustness to *population* shift?

$\Longrightarrow$ *Recent* VinDr-Mammo vs. *old* DDSM;

$\Longrightarrow$ Analysis with anisotropy-sensitive tools (Biermé *et al.*, 2025, *Appl. Comput. Harmon. Anal.*)

$\Longrightarrow$ Hurst and anisotropy-based segmentation (Davy *et al.*, 2026, *Preprint*)

Goal: advance computed-aided tools for breast cancer *prevention* and *detection* with *interpretable* X-ray image analysis procedures.